Solar Energy 301 (2025) 113933

Contents lists available at ScienceDirect

Solar Energy

journal homepage: www.elsevier.com/locate/solener

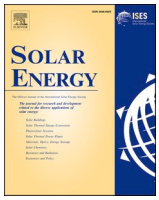

Mechanism-guided design and process optimization of a roll-to-sheet coating system for flexible perovskite solar cells

Hou-Chin Cha [a,b], Ssu-Yung Chung [c], Shih-Han Huang [b], Chia-Feng Li [c,d], Shun-Wei Liu [a,b,e,*], Yu-Ching Huang [b,c,e,f,*]

[a] College of Engineering, Ming Chi University of Technology, New Taipei City 243303, Taiwan
[b] Organic Electronics Research Center, Ming Chi University of Technology, New Taipei City 243303, Taiwan
[c] Department of Materials Engineering, Ming Chi University of Technology, New Taipei City 243303, Taiwan
[d] Department of Materials Science and Engineering, National Taiwan University, Taipei 10617, Taiwan
[e] Center for Sustainability and Energy Technologies, Chang Gung University, Taoyuan 33302, Taiwan
[f] Research Center for Critical Issues, Academia Sinica, Taipei 115201, Taiwan

ARTICLE INFO

Keywords:
R2S slot-die coating
Flexible
Heated roller-assisted coating
Two-step deposition
Large-area processing

ABSTRACT

We report a mechanism-informed roll-to-sheet (R2S) slot-die coating system engineered for high-uniformity deposition on large-area flexible substrates, advancing scalable fabrication of perovskite solar cells (PSCs). Unlike conventional post-deposition thermal treatments, which induce secondary fluid flow and result in pinholes, thickness non-uniformity, and compromised interfacial contact, our R2S platform integrates an in-line heated roller that delivers precise thermal energy during coating. This real-time thermal input governs solvent evaporation kinetics and crystallization pathways, minimizing defect formation at the wet-to-dry transition stage. Guided by a detailed understanding of solvent drying dynamics and their influence on film morphology, we optimized critical parameters, including roller temperature, rotation speed, and solution flow rate, to achieve highly uniform and pinhole-free active layers. Devices fabricated with two R2S-coated functional layers exhibited a power conversion efficiency (PCE) of 12.58 %, while triple-layer R2S devices reached 11.58 %, approaching the 13.24 % PCE benchmark of spin-coated controls. Notably, the integrated heated roller not only accelerates drying but also enhances film adhesion and crystallinity, enabling reproducible multi-layer stacking with superior mechanical integrity. This scalable R2S approach bridges the gap between lab-scale coating and industrial roll-to-roll production, laying essential groundwork for future high-throughput manufacturing of flexible PSCs.

1. Introduction

With the rapid advancement of renewable energy technologies, perovskite solar cells (PSCs) have garnered significant attention due to their high power conversion efficiency (PCE), low manufacturing cost potential, and wide-ranging application prospects. Understanding the structural stability of perovskite materials is essential for advancing device performance, especially in flexible and large-area applications. Recent work by Sekar et al. [1] provides a comprehensive discussion of the Goldschmidt tolerance factor and octahedral factor across various perovskite compositions, offering valuable insights into phase formability and compositional stability, which serve as important guidelines for rational material selection. In particular, flexible PSCs (F-PSCs) have emerged as a key enabling technology for portable energy devices, wearable electronics, and building-integrated photovoltaics (BIPV) [2,3]. To achieve the commercial viability of PSCs, especially for large-area production on flexible substrates, scalable roll-to-roll (R2R) coating processes are essential. Although R2R systems may involve significant initial capital costs depending on equipment scale, recent studies have demonstrated their capability to deliver uniform and high-performance perovskite films through precise control of coating parameters and thermal management. For instance, Angmo et al. [4] reported the fully R2R fabrication of perovskite modules with printed carbon electrodes, achieving PCEs up to 15.5 % for individual small-area cells and 11.0 % for large-area modules. The study emphasized robust process control and reproducibility across 1,600 cells under ambient conditions. Similarly, Kim et al. [5] demonstrated pilot-scale, fully R2R manufacturing of flexible PSCs using gravure printing and an eco-friendly antisolvent

* Corresponding authors.

https://doi.org/10.1016/j.solener.2025.113933
Received 6 May 2025; Received in revised form 14 August 2025; Accepted 25 August 2025
Available online 27 August 2025

bathing process. Their process yielded PCEs of 13.8 % for fully R2R-processed devices, with excellent wet film uniformity and wide processing tolerance. Othman et al. [6] applied hot-deposition R2R slot-die coating to fabricate triple-cation perovskite films in ambient air, achieving stabilized efficiencies up to 12 %—the highest for inverted R2R PSCs—by engineering the HTL interface and optimizing crystallization dynamics. Finally, Weerasinghe et al. [7] validated the scalability of R2R systems using industrial printing tools to fabricate large-area modules under ambient conditions, confirming film consistency across production batches. These studies collectively establish that modern R2R platforms can deliver reproducible, uniform perovskite layers suitable for high-efficiency, scalable solar modules. In the R2R slot-die coating process for PSCs, substrate selection plays a pivotal role, especially considering the need for flexibility and low-temperature processability. Flexible substrates must withstand processing temperatures below 150 °C to avoid deformation—an especially important consideration for large-area manufacturing [8]. Commonly used materials such as polyethylene terephthalate (PET) and polyethylene naphthalate (PEN) are favored for their low cost, excellent flexibility, and high optical transparency [9]. However, despite the widespread use of PET and PEN in printed electronics, their relatively low intrinsic glass transition temperatures (PET: ~70 °C, PEN: ~120 °C) may lead to thermal deformation under prolonged heating. Although commercial PET and PEN substrates can tolerate processing temperatures up to ~150 °C and ~180 °C, respectively, such high-temperature treatments are typically applied for short durations (often less than 10 s) under N_2 flow to accelerate solvent evaporation and minimize thermal stress [10]. To address this, Skafi et al. developed a process enabling stable F-PSCs fabrication on PET at ≤100 °C, while Chen et al. demonstrated successful processing on PEN at 120 °C [11]. For applications requiring higher thermal stability, polyimide (PI) substrates—which operate across a broad temperature range from −200 °C to 400 °C—are a viable option, albeit with drawbacks such as low transparency and higher cost [12]. Transparent polycarbonate (PC) substrates offer good thermal resistance but are incompatible with common perovskite solvents, limiting their applicability in F-PSCs [13]. Beyond substrate considerations, optimization of carrier transport layers and interfacial structures is also critical to enhancing the stability and efficiency of flexible PSCs. For example, Galagan et al. demonstrated slot-die coating of SnO_2 and perovskite layers on 30 cm-wide flexible substrates under ambient conditions (25 °C/60 % RH), achieving a certified PCE of 13.5 % for small-area devices. While these devices were not fabricated across the full substrate width, the result serves as a valuable proof of concept and a meaningful step toward the scalable development of flexible perovskite solar cell technologies [14]. Dou et al. used flexible glass substrates and spin-coated spiro-OMeTAD atop SnO_2/perovskite layers to reach 14.1 % efficiency [15], while Kim et al. employed PEDOT:PSS as the hole transport layer and achieved approximately 11.0 % efficiency in their R2R-fabricated perovskite solar cells [16]. Interfacial engineering has also played a key role in performance improvement during R2R fabrication. For instance, Ochoa et al. used PEIE to modify the SnO_2 surface, reducing defect density and raising efficiency to 15.8 % [17], while Hwang et al. developed a two-step perovskite deposition process incorporating minor cations into the PbI_2 layer and utilized gas-quenching in an enclosed space to assist MAI infiltration and complete perovskite conversion. Devices were fabricated on ZnO substrates using fully printed layers except for the top electrode, achieving a PCE of 11.96 % [18]. Meanwhile, efforts to improve the active layer in R2R processing have led to further gains—Li et al. used a $Pb(Ac)_2$-based precursor in a GBL:DMSO solvent system to fabricate films with 17.2 % efficiency [19], and Zhang et al. achieved 18.3 % efficiency using PbI_2-DMSO solutions to form highly crystalline perovskite films [20].

Despite significant advances in processing technologies, film formation still presents major challenges, particularly in the control of solvent evaporation rates and crystallization behavior. In most current R2R manufacturing processes, crystallization is primarily driven by post-deposition thermal treatments such as infrared or oven heating. However, these methods often result in delayed solvent evaporation and unstable crystallization dynamics. In addition, the continuous motion of the substrate can lead to redistribution of the coating solution, causing non-uniform film morphology, the formation of pinhole defects, and poor interfacial contact, all of which negatively impact device performance and reproducibility. Our previous studies have demonstrated that during R2R processing, the early-stage crystallization of polymers as the film transitions from a wet to a dry state plays a crucial role in morphology control and the formation of an optimal bulk heterojunction (BHJ) structure [21]. This initial crystallization behavior is highly sensitive to thermal and airflow conditions during the drying process, while the final degree of crystallinity and phase separation can be further adjusted through thermal annealing. These findings provide valuable insight into how drying and post-treatment conditions work in tandem at different stages to shape the final film structure and influence device performance. In our study on slot-die coating of perovskite active layers, we observed that the early transition from wet to dry film significantly affects the final film morphology. During this process, solvent evaporation drives the rapid formation of intermediate crystallites in the wet stage. As evaporation continues, molecular diffusion slows, halting further crystal growth. Although the crystallites appear stable, they remain metastable and undergo structural rearrangement aided by residual solvent. This suggests that solvent evaporation rate critically influences crystal evolution and final film quality [22]. Based on our understanding of the film formation mechanism during the solution process, we developed a low-cost, continuous manufacturing system (MK-20) for large-area perovskite solar cells [23]. This system integrates slot-die coating and fast thermal processing (FTP), allowing precise control over solvent evaporation and crystallization behaviors. The insights into wet-to-dry film transitions guided the optimization of processing parameters, enabling uniform film quality, high yield, and reliable device performance.

Building on this understanding of wet-film-to-dry-film dynamics, we have collaborated with Vestech Technology Co. (Taiwan) to co-develop a localized roll-to-sheet (R2S) coater, model W17RD15, utilizing slot-die coating. A key feature of this system is the integration of a heated roller that enables localized, progressive thermal energy during coating. This design allows for real-time solvent management and crystallization guidance, promoting uniform film formation and reducing defect density. The platform also offers scalability for future upgrade to continuous R2R production. Given the sensitivity of flexible substrates, achieving uniform deposition and controlled solvent evaporation is crucial to maintaining high film quality and device performance. The system is also compatible with rapid post-treatment methods such as intense pulsed light (IPL) [24] and near-infrared (NIR) heating [25,26], which are effective in accelerating perovskite crystallization and enhancing device performance. Furthermore, the entire process can be carried out under ambient conditions without the need for costly high-vacuum systems, significantly reducing manufacturing and operational costs. Compared to imported equipment, this localized platform offers a cost-effective and highly customizable solution for flexible PSC development.

2. Development and implementation of heated-roller slot-die coating

2.1. In-house design and localized manufacturing (W17RD15)

To reduce costs and save space, we have developed a flexible perovskite solar cell processing system with the following key features:

(a) Versatile processing environment – The system features a compact design (680 × 640 × 716 mm) that minimizes space requirements, making it easy to integrate into various work environments. While optimized for coating processes in ambient conditions, its small size allows for easy placement in controlled

environments such as clean rooms or specialized enclosures to meet specific processing requirements. This flexibility ensures adaptability to different operational needs while maintaining process stability when handling moisture- and oxygen-sensitive materials. Additionally, its portability facilitates seamless integration into existing laboratory setups without requiring significant modifications. The system's dimensions are illustrated in Fig. 1.

(b) Minimal material consumption – The system allows for thin-film parameter optimization using minimal solution volumes. With its high-precision coating mechanism, experiments can be performed using just hundreds of microliters (μL) of solution, maximizing material utilization efficiency. For example, when operating at a coating speed of 1.2 m/min with a solution flow rate of 1.2 mL/min, coating a 25 cm substrate requires only 0.3 mL (300 μL) of solution. This feature is particularly beneficial for developing and optimizing high-cost or rare materials.

(c) Integrated heated roller – The system incorporates a heated roller capable of reaching up to 200 °C, ensuring rapid drying of wet films and enhancing processing efficiency. The roller features five evenly distributed heating rods, providing uniform heat distribution to accelerate drying, minimize solvent residue effects, and improve film uniformity.

(d) Modular expandability – The system is designed for expandability, enabling the integration of additional modules to meet specific processing requirements. Possible expansions include NIR or IPL rapid annealing, air-assisted coating technology for enhanced film uniformity, UV curing for specialized polymer layers, and plasma treatment for improved surface energy and film adhesion. These options provide enhanced process flexibility, enabling optimization for different material systems and device architectures.

(e) Reduced dependence on imported equipment – Enhances local manufacturing capabilities while mitigating risks related to supply chain restrictions or technology access barriers. By independently developing critical processing technologies, we reduce reliance on foreign equipment, minimizing risks associated with supply chain disruptions or technology embargoes. Furthermore, the system's modular design enables local teams to handle maintenance and upgrades, reducing downtime, lowering long-term operational costs, and improving overall equipment availability and production efficiency.

2.2. Slot-die coating with integrated heated roller

This study will primarily focus on the development of a slot-die coating process integrated with a heated roller. Slot-die coating is a one-dimensional, non-contact deposition technique that delivers a continuous flow of solution between the slot-die head and the substrate, enabling precise control over the coating width. The system's heated roller, capable of reaching up to 200 °C, ensures rapid drying of wet films, improving processing efficiency and film uniformity. By carefully controlling the flow rate, slot-die coating minimizes material waste, making it an efficient process. The final dry film thickness can be estimated using the following equation, based on specific coating speed, feed rate, coating width, and solid content in the solution:

$$d = \frac{fc}{Sw\rho}$$

where d represents the dry film thickness, f is the feed flow rate, S is the coating speed, w is the coating width, c is the solid content in the solution, and ρ is the density of the dried material. In a conventional R2R slot-die coating process (as shown in Fig. 2(a)), after the solution is applied, the coated substrate is transported horizontally into an oven where it is heated to remove the solvent. This process is depicted in Fig. 2(b). As the temperature increases, the viscosity of the solution decreases, which may cause secondary flow during the heating process. As heating continues over time, the solvent gradually evaporates (solvent removal), causing the solution to harden until it eventually solidifies. Moreover, the addition of an external oven also increases the overall space of the coating equipment. In contrast, the R2S slot-die coating process designed in this study (as shown in Fig. 2(c)) operates

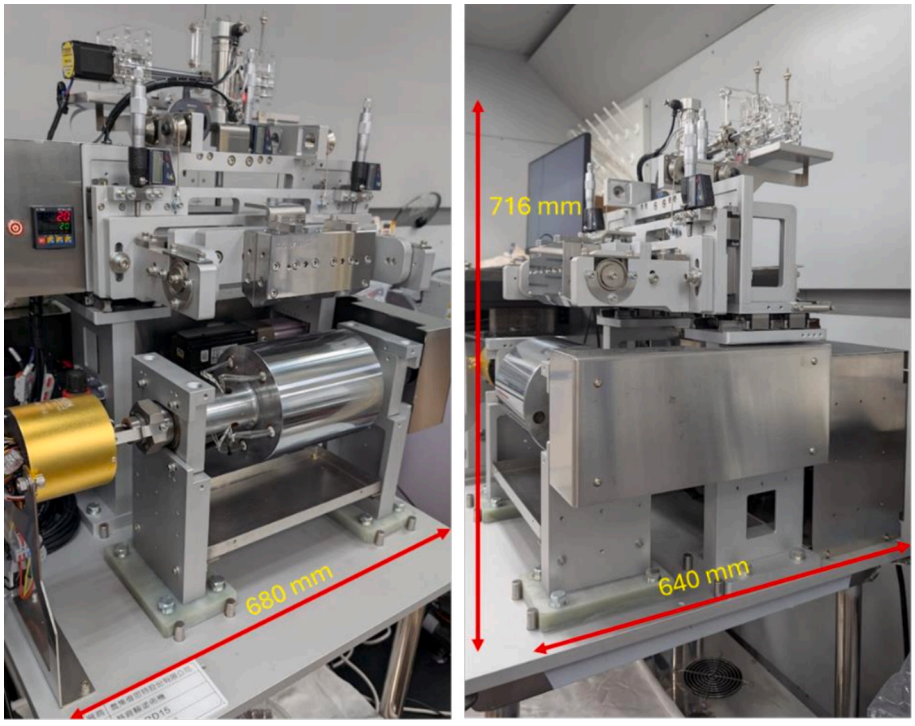

Fig. 1. Dimensions of the roll-to-sheet coating system (W17RD15), highlighting its compact design (680 × 640 × 716 mm), which makes it ideal for integration into various work environments, including controlled settings.

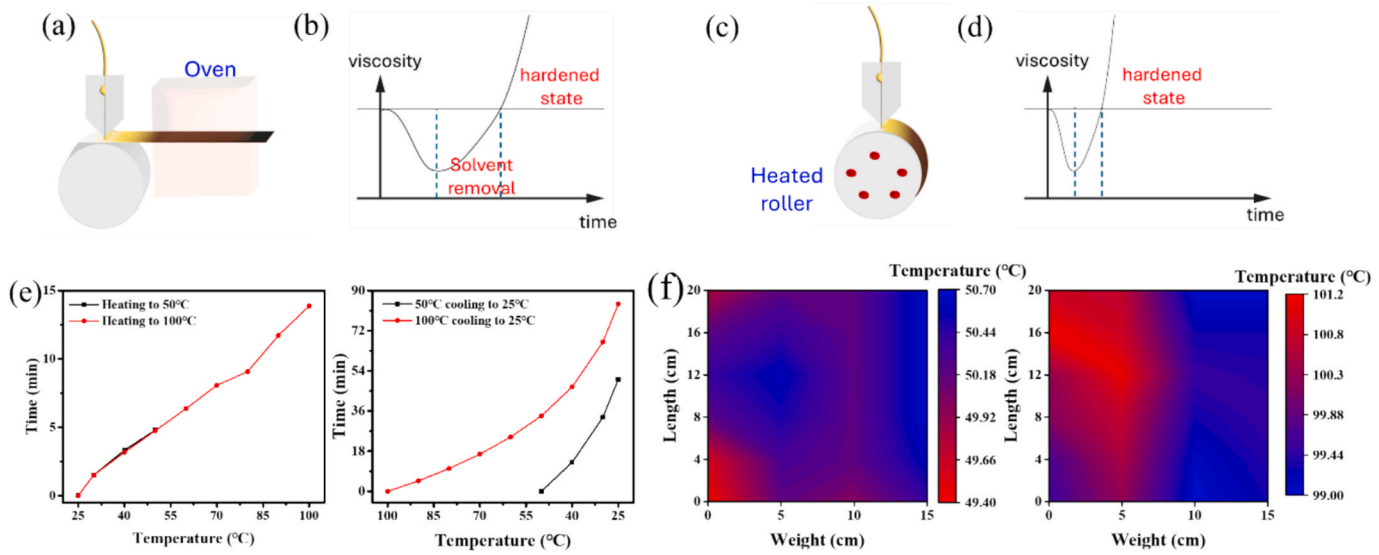

Fig. 2. Comparison of conventional R2R slot-die coating and the R2S slot-die coating process. (a) Conventional R2R slot-die coating, where the coated substrate is horizontally transported to an oven for solvent removal. (b) Solvent removal process in conventional R2R slot-die coating. (c) The R2S slot-die coating process, where the substrate is directly applied to a heated roller. (d) Solvent removal process using a heated roller in R2S slot-die coating. (e) Heating and cooling curves of the heated roller. (f) Surface temperature uniformity of the heated roller at 50 °C and 100 °C, respectively.

differently. In this method, the substrate is directly adhered to a heated roller, accelerating the heating and solvent-removal process, allowing for a faster transition to the hardened state (as illustrated in Fig. 2(d)). This design is based on our understanding of the wet-to-dry transition mechanism, where timely and directional solvent evaporation is critical for controlling film morphology and crystallization behavior. Unlike the traditional method in R2R slot-die coating, the R2S process does not transport the solution horizontally after coating. Instead, it completes the initial drying in a shorter time. This design effectively prevents secondary flow during the heating process, thus maintaining the uniformity of the coating layer. To further validate the thermal management capability of our R2S system, we characterized the heating rate, temperature uniformity, and cooling performance of the heated roller. As shown in Fig. 2(e), the temperature–time profile reveals a heating rate of 5.2 °C/min. In terms of cooling, we addressed the typical challenge of prolonged cooling durations in heated drum systems by implementing a hybrid strategy. Once the roller reaches the target temperature, it is cooled by forced air convection through a strategically positioned array of fans surrounding the drum. This approach reduces the total cooling time to under 45 min, enabling the roller to reach a safe handling temperature below 45 °C, which is significantly faster than conventional systems that often require several hours to cool. Additionally, the surface temperature uniformity was assessed at both 50 °C and 100 °C, as shown in Fig. 2(f), with results indicating a variation within ±1.5°C across the roller surface. This uniformity is sufficient to support high-quality thin-film deposition and highlights the practical advantages of our system-level design for rapid and consistent perovskite film formation.

3. Experimental sections

3.1. Materials

Poly(3,4-ethylenedioxythiophene):poly(styrenesulfonate) (PEDOT:PSS) (Clevious P VP AI 4083) was obtained from Heraeus Ltd.. Formamidinium Iodide (FAI, 99.99 %) and methylammonium chloride (MACl, 99.99 %) were purchased from Greatcell solar materials. Cesium iodide (CsI, 99.99 %), dimethyl sulfoxide (DMSO, 99.9 %), dimethylformamide (DMF, ≥99.9 %), chlorobenzene (CB, 99.9 %), isopropanol (IPA, 99.5 %) and polyethylenimine (PEI, >99 %) were purchased from Sigma-Aldrich. Lead iodide (PbI_2, 99.99 %) was purchased from TCI. $PC_{61}BM$ was purchased from Lumtec. All the chemicals were used without further purification. 2-Thiopheneethylamine, hydrochloride (TEACl) solution was purchased from FrontMaterals Ltd. (FMPV).

3.2. Preparation of precursor solutions for R2S coating

The PEDOT:PSS ETL (~12 nm thick) was prepared by spin-coating a PEDOT:PSS solution containing 90 wt% isopropanol (IPA). The 1.0 M inorganic solution, consisting of 1.0 mmol PbI_2 doped with 5 mol% CsI, was dissolved in a 1 mL DMF:DMSO co-solvent mixture (9:1 vol%). The inorganic solution was stirred at 70 °C overnight. The organic salt solution, containing 0.37 M FAI and 0.1 M of the MACl mixture with different molar ratios, was dissolved into IPA and stirred for 3 h. A 4 mM TEACl dissolved in 1 ml IPA. The PCBM solution with 20 mg dissolved in 1 ml CB. A 0.1 wt% PEI solution dissolved in 1 ml IPA.

3.3. Device fabrication

The structure of the PSCs was PET/ITO/PEDOT:PSS/Perovskite/TEACl/PCBM/PEI/Ag, As shown in Fig. 3. The R2S-coated PSCs were fabricated using an automated R2S equipment (Vestech Taiwan Corporation). Firstly, the ITO substrates were treated with UV-ozone for 30 min. The wet film of PEDOT:PSS, hole transport layer (HTL), was processed by roller at 70 ℃, with a coating speed of 0.5 m min^{-1} and a flow rate of 0.5 ml min^{-1}. The PEDOT:PSS film was then obtained by annealing at 120 ℃ for 12 min. The perovskite layer was prepared by using a sequential deposition method. The PbI_2:CsI layer was first R2S-coated with a R2S head spacing of 200–250 μm. The coating parameters were set at 60℃, a coating speed of 1.2 m min^{-1} and a flow rate of 1.1 ml min^{-1}. The wet film was dried on the roller for 1 min. The FAI:MACl film was subsequently slot-die coated onto the PbI_2:CsI layer at a substrate temperature of 60 ℃, a coating speed of 1.2 m min^{-1} and a flow rate of 1.1 ml min^{-1}. The as-prepared perovskite films were then annealed at 100 ℃ for 15 min. All steps above were carried out under ambient conditions without the need for an inert atmosphere, with the relative humidity (RH) controlled at 40–60 % and monitored using a calibrated hygrometer. Next, the large-area PSC is cut into 2 × 2-sized substrates. Then, the TEACl solution was spin-coated at 3000 rpm for 20

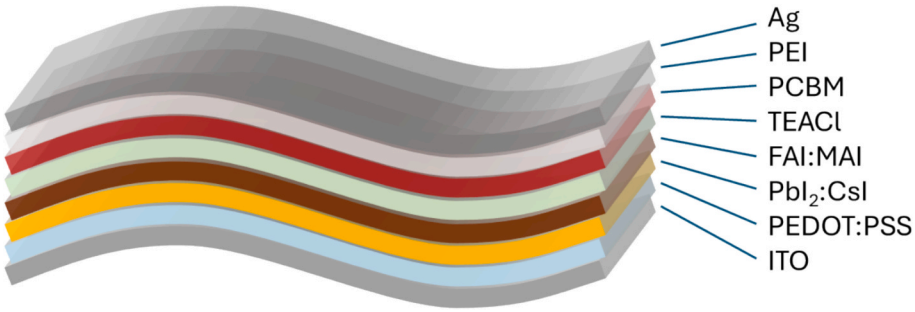

Fig. 3. Schematic diagram of flexible perovskite solar cell structure.

s and annealed at 150 °C for 40 s to enhance interaction with the perovskite surface. The $PC_{61}BM$ solution was spin-coated at 1000 rpm for 30 s, ensuring the formation of a smooth and well-connected ETL for efficient electron extraction. The PEI solution was spin-coated at 3000 rpm for 30 s, enhancing energy level alignment. Finally, a 120 nm Ag electrode was deposited through thermal evaporation under a vacuum of 2×10^{-6} torr. All the device areas used in this study are 0.09 cm^2.

3.4. Characterization

The current–voltage characteristics of the devices were measured using a Keithley 2410 source meter under 100 mW cm^{-2} illumination from an AM 1.5 solar simulator (YSS-150A, Yamashita Denso). The external quantum efficiency (EQE) spectrum and the corresponding integrated current density were measured using a quantum efficiency measurement system (Enlitech, QE-R). The crystal structure of the perovskite films was analyzed by X-ray diffraction (XRD) using a Rigaku TTRAX III diffractometer. Steady-state photoluminescence (PL) measurements were carried out using a fluorescence spectrophotometer (FluoroMax-4, HORIBA). The perovskite surface morphology was measured by atomic force microscopy (AFM) (XE7, Park Systems).

4. Results and discussion

Initially, we fabricated perovskite solar cells on a flexible substrate using a full spin-coating process to serve as a reference device. The fabrication process began with the deposition of the hole transport layer onto the flexible substrate via spin coating. Although PEDOT:PSS is widely used as a HTL in rigid perovskite solar cells due to its excellent conductivity and optical transparency, its application in two-step perovskite deposition on flexible PET/ITO substrates remains extremely limited. This is primarily due to several intrinsic challenges, including surface wettability mismatch between PEDOT:PSS and PbI_2 precursors, which leads to poor nucleation and film uniformity during the first step, as well as its hydrophilic nature and relatively low chemical stability under prolonged contact with polar solvents, which exacerbate degradation during ambient processing. Despite these limitations, our study demonstrates a reproducible and scalable two-step coating process directly on flexible PET/ITO/PEDOT:PSS substrates, achieving uniform film formation and competitive device performance. To the best of our knowledge, this represents one of the first successful implementations of a two-step p–i–n structured perovskite solar cell using PEDOT:PSS on a flexible platform. To contextualize our achievement, Table S1 presents a comparative summary of representative flexible perovskite solar cells (F-PSCs) and flexible perovskite solar modules (F-PSMs) fabricated by slot-die coating, listing device architectures, active areas, and key photovoltaic parameters. Compared with reported works, our approach offers not only ambient process compatibility and mechanical flexibility but also a viable pathway for low-temperature, large-area manufacturing. This table further highlights the novelty and relevance of our PEDOT:PSS-based two-step device structure within the landscape of flexible perovskite photovoltaics. We selected PEDOT:PSS as the HTL for its water-based nature, making it highly suitable for ambient processing. This characteristic not only simplifies the fabrication process and reduces environmental impact but also enables low-temperature, scalable manufacturing on flexible substrates. For the perovskite layer, we adopted a two-step deposition method. In the first step, an inorganic precursor layer was deposited onto the HTL. This was followed by the deposition of the organic solution in the second step. After these two layers were applied, a thermal annealing process was conducted to promote crystallization. This step is crucial for achieving high-performance perovskite solar cells, as a well-formed crystalline structure enhances light absorption and facilitates charge carrier transport. The overall distribution of photovoltaic characteristics under different processing conditions is illustrated in Fig. 4, providing a comprehensive comparison of device performance variations. The photovoltaic characteristics of these reference devices are summarized as follows: an average open-circuit voltage (V_{OC}) of 1.07 ± 0.06 V, a short-circuit current density (J_{SC}) of 16.95 ± 1.34 mA/cm^2, a fill factor (FF) of 55.14 ± 4.48 %, and a power conversion efficiency of 10.00 ± 1.13 %. The highest recorded values reached 1.09 V for V_{OC}, 19.55 mA/cm^2 for J_{SC}, 61.81 % for FF, and 13.24 % for PCE, as listed in Table 1. We further investigated the variation in series resistance (Rs) and shunt resistance (Rsh) of PSCs processed under heated rollers at different temperatures. Commonly, high-performance devices exhibit low Rs and high Rsh. From the results, a noticeable drop in PCE was observed when the processing temperature increased to 65 °C, primarily attributed to the increased Rs and decreased Rsh. A higher Rs suggests that elevated temperatures may damage the contact between the inorganic layer and the bottom electrode, thereby increasing interfacial impedance and hindering charge transport in flexible PSCs.

To optimize the process and enhance scalability, we later replaced the traditional spin-coating method with the slot-die coating process, implemented using our custom-designed R2S machine (W17RD15). This modification was first applied to the HTL and the inorganic precursor layer of the perovskite film (the first step in the two-step deposition process), while the deposition methods for the other functional layers remained the same as in the reference samples. In this process, controlling the temperature of the roller is critically important. The R2S system is equipped with adjustable roller heating rods that accelerate solvent evaporation, effectively controlling the drying rate of the film and ensuring uniformity and crystallization quality. Compared to the spin-coating process, slot-die coating offers more precise control over film thickness and solvent evaporation, leading to improved film uniformity and reducing material waste. To systematically investigate the impact of roller heating on film quality, we varied the roller temperature during the first-step deposition and analyzed its effect on device performance. The best results were obtained at 55 °C, where the devices exhibited an average V_{OC} of 0.88 ± 0.18 V, J_{SC} of 22.69 ± 1.13 mA/cm^2, FF of 48.45 ± 7.85 %, and PCE of 9.95 ± 2.76 %. The distribution of device parameters under different heating conditions is illustrated in Fig. 4 and listed in Table 1. The highest recorded values for V_{OC}, J_{SC}, FF, and PCE at this temperature were 0.97 V, 22.88 mA/cm^2, 56.79 %, and 12.58 %, respectively. Compared to the reference device (full spin-

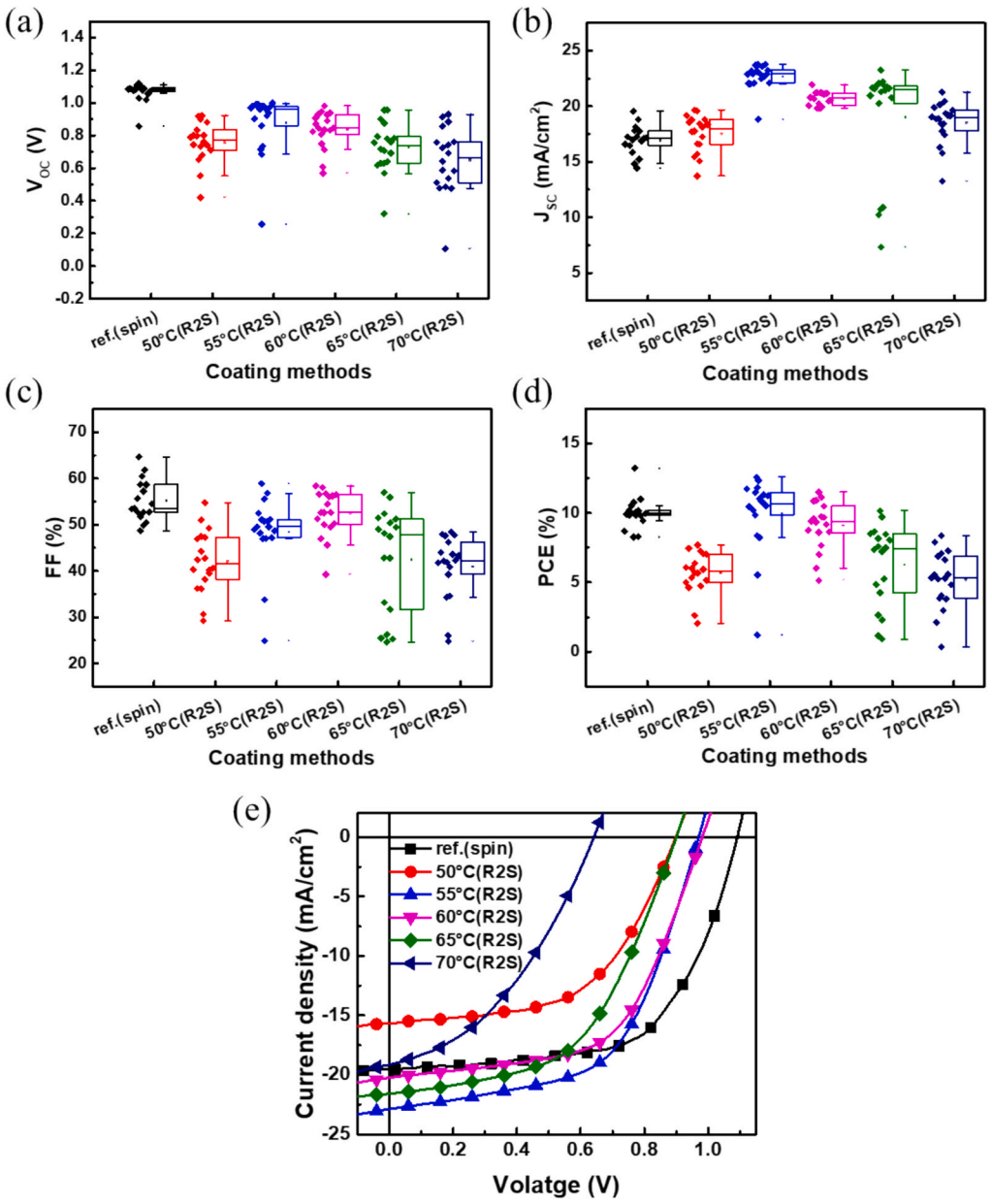

Fig. 4. The image shows the electrical characteristics of devices fabricated using different coating methods, including R2S-coated devices with heated rollers at various temperatures (50 °C, 55 °C, 60 °C, 65 °C, and 70 °C) when fabricating step one and spin-coated reference devices. It includes open-circuit voltage (a), short-circuit current density (b), fill factor (c), and power conversion efficiency (d), along with the corresponding current density–voltage (J-V) curves (e) for the device with the highest recorded power conversion efficiency.

coating process), the R2S-coated devices at 55 °C demonstrated a significant improvement in J_{SC}, while V_{OC} and FF were slightly reduced. The increase in J_{SC} suggests improved light absorption and charge collection, likely due to the better film uniformity achieved through the R2S process. However, the slight decrease in V_{OC} and FF indicates that further optimization of the perovskite crystallization and interface quality is necessary. Despite these variations, the highest recorded PCE (12.58 %) under the optimized R2S conditions approached the peak performance of the reference device (13.24 %), highlighting the potential of the slot-die coating method for scalable perovskite solar cell fabrication.

In the two-step fabrication of perovskite layers, precise control over the thickness and uniformity of the inorganic layer is crucial for achieving optimal crystallization of the organic layer. An excessively thick inorganic layer can hinder the infiltration of the organic layer, leading to poor interfacial contact and reduced efficiency. On the other hand, an overly thin layer may not provide sufficient electron transport pathways, limiting carrier mobility. The R2S slot-die coating technique enables precise deposition control, which is advantageous for large-area processing. Moving forward, further refinements in temperature control, deposition speed, and solvent concentration will be key to improving film quality and achieving ideal perovskite crystallization. We further applied the R2S slot-die coating process to deposit the organic layer, alongside the HTL and inorganic layers, as shown in Fig. 5. The resulting films exhibited excellent uniformity and precision, demonstrating the significant advantages of this technique for large-area processing. Fig. 6 (a)-(b) illustrates the distribution of photovoltaic parameters under different flow rates during organic layer deposition, while the corresponding device characteristics are summarized in Table 2. As the flow rate increases, the PCE, V_{OC}, J_{SC}, and FF all improve. The best results were obtained at a flow rate of 1.1 mL/min, where the devices achieved an average V_{OC} of 0.99 ± 0.05 V, J_{SC} of 20.70 ± 0.43 mA/cm^2, FF of

Table 1
The table presents the photovoltaic characteristics of devices fabricated using different coating methods, including average and highest recorded values based on 18 devices. The coating methods include spin-coated (reference) and R2S-coated devices for step one with heated rollers at various temperatures (50 °C, 55 °C, 60 °C, 65 °C, and 70 °C) when fabricating step one. Each average value is accompanied by its standard deviation, highlighting the consistency across the measurements.

Coating method (inorganic layer)		V_{OC} (V)	J_{SC} (mA/cm^2)	FF (%)	PCE (%)	Rs (Ω)	Rsh (Ω)
Spin-coated (ref.)		1.09	19.55	61.81	13.24		
		1.07 ± 0.06	16.95 ± 1.34	55.14 ± 4.48	10.00 ± 1.13		
R2S-coated	50℃	0.90	15.67	54.75	7.70	223.87 ± 78.38	1096.82 ± 587.19
(Heated Roller)		0.76 ± 0.13	17.52 ± 1.68	42.06 ± 6.74	5.66 ± 1.53		
	55℃	0.97	22.88	56.79	12.58	142.52 ± 28.94	1861.99 ± 844.39
		0.88 ± 0.18	22.69 ± 1.13	48.45 ± 7.85	9.95 ± 2.76		
	60℃	0.98	20.23	58.06	11.51	152.11 ± 48.42	2365.87 ± 1409.98
		0.83 ± 0.11	20.70 ± 0.63	52.43 ± 4.98	9.09 ± 1.74		
	65℃	0.90	21.59	52.38	10.16	286.24 ± 308.64	2219.48 ± 1196.68
		0.73 ± 0.15	19.00 ± 5.15	42.47 ± 11.44	6.26 ± 2.93		
	70℃	0.86	20.43	47.79	8.37	172.68 ± 65.76	830.02 ± 401.43
		0.65 ± 0.20	18.52 ± 1.90	40.93 ± 6.95	5.17 ± 2.08		

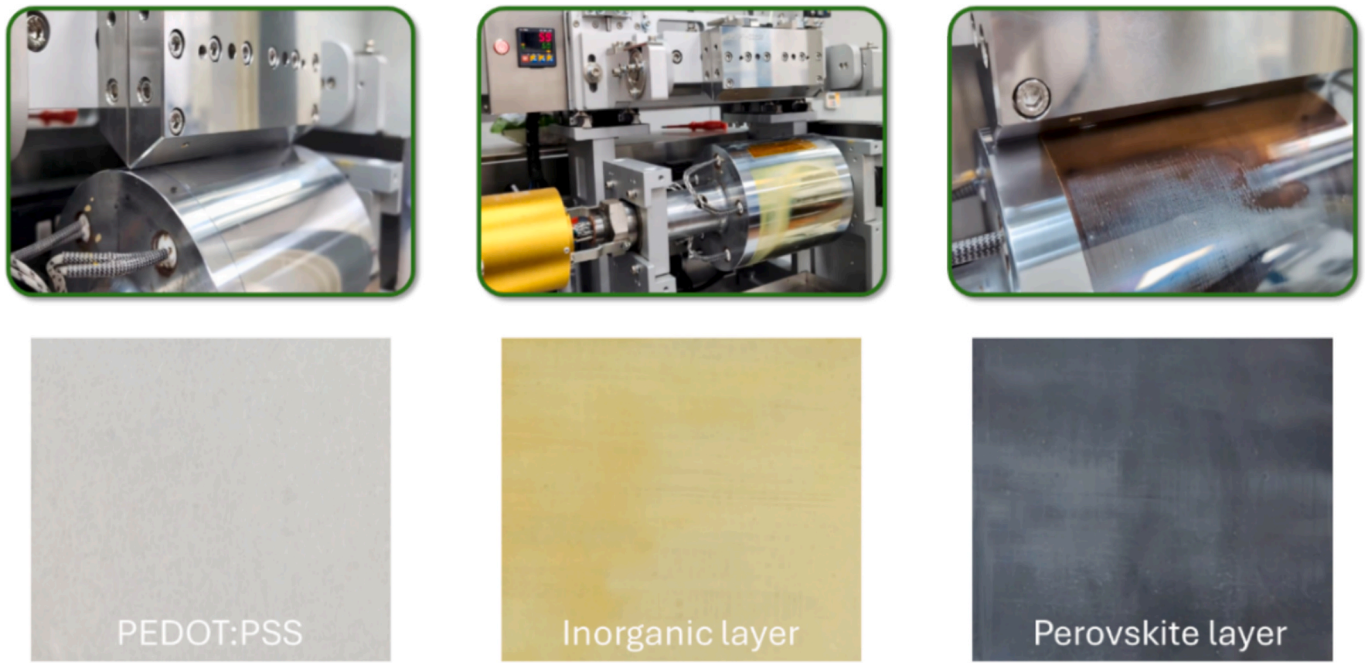

Fig. 5. The image illustrates the film layers fabricated using the R2S coating technique, including the PEDOT:PSS layer (hole transport layer), the inorganic layer, and the perovskite layer. It also shows the appearance of the completed film layers after coating, highlighting their smooth and uniform surface.

48.70 ± 4.25 %, and PCE of 10.02 ± 0.99 %. The peak performance was observed with a PCE of 11.58 %, V_{OC} of 0.96 V, J_{SC} of 20.88 mA/cm^2, and FF of 57.68 %. In addition, we investigated the variation in Rs and Rsh under different flow rates. At lower flow rates, the limited availability of organic salts led to incomplete conversion of PbI_2, especially near the bottom interface. This incomplete reaction resulted in increased Rs, due to poor interfacial contact, and decreased Rsh, attributed to defect-induced leakage paths. As the flow rate increased, the excess organic solution facilitated a more complete reaction with the inorganic layer, enabling full perovskite conversion. This improved conversion yielded lower Rs and higher Rsh, indicative of enhanced interfacial quality and more efficient charge transport. These electrical characteristics are consistent with the improvements observed in the overall device performance. We checked the external quantum efficiency (EQE) spectrum of PSCs fabricated under varying flow rates. As shown in Fig. 6 (c), the EQE curves exhibit a clear upward shift with increasing flow rates. Specifically, when the flow rates exceeds 0.5 mL/min, a significant improvement in the EQE response is observed in the 300–500 nm wavelength range, suggesting that the inorganic bottom layer is more fully converted into the perovskite phase. This enhancement increases the integrated area under the EQE curve and the simulated current density, which aligns well with the measured J_{SC} values. X-ray diffraction (XRD) analysis of the second step deposition at varying flow rates, shown in Fig. 6(d), indicates that PbI_2 peaks are no longer present at flow rates above 0.9 mL/min, confirming the complete conversion to perovskite. Closer inspection of the XRD patterns reveals that PbI_2 reflections reappear at flow rates of 1.1 and 1.3 mL min^{-1}, indicating incomplete conversion under these conditions. In addition, a minor peak near 10° (2θ) is observed at lower flow rates, consistent with δ-phase perovskite (δ-$FAPbI_3$) or low-dimensional phases such as FA_3PbI_5. These optoelectronically inactive phases are likely associated with insufficient infiltration and reaction of organic salts at sub-optimal flow, and their presence correlates with the degraded device performance measured at these conditions. However, at a flow rate of 1.3 mL/min, while V_{OC}, J_{SC}, and FF stabilize, the PCE drops slightly to 10.79 %, suggesting diminishing returns at higher flow rates. To further investigate the effect of precursor flow rate during the second-step coating on perovskite film quality, steady-state photoluminescence (PL) spectra were measured under various flow conditions, as shown in Fig. 6(e). The PL results show a clear trend: increasing the flow rate from 0.5 to 1.1 mL/min leads to a

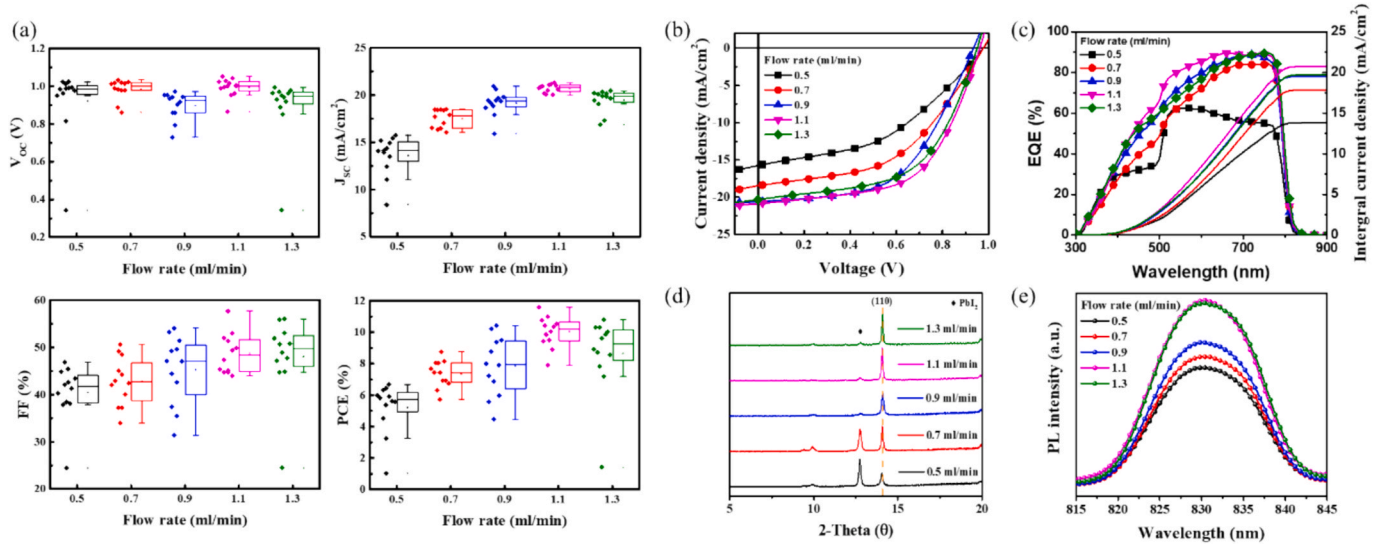

Fig. 6. The image shows the electrical characteristics of devices fabricated using the two-step perovskite method, with the second perovskite layer applied at different flow rates. It includes (a) Device performance distribution, along with the corresponding current density–voltage (J-V) curve (b) for the device with the highest recorded power conversion efficiency.(c) EQE spectra and the corresponding integrated J_{SC} values. (d) The X-ray diffraction (XRD) images corresponding to each of the parameters. (e) PL spectra of perovskite films coated using the R2S process at different second-step flow rates.

Table 2
The table presents the electrical characteristics of devices fabricated using different flow rates during step 2 of the two-step perovskite deposition. The flow rates tested include 0.5, 0.7, 0.9, 1.1, and 1.3 mL/min. The table includes average and highest recorded values based on 12 devices, with each average value accompanied by its standard deviation. This highlights the consistency across the measurements.

Flow rate (ml/min) (organic layer)	V_{OC} (V)	J_{SC} (mA/cm^2)	FF (%)	PCE (%)	Rs (Ω)	Rsh (Ω)
0.5	0.98 0.92 ± 0.19	15.76 13.59 ± 2.10	43.10 40.46 ± 5.83	6.68 5.21 ± 1.61	420.56 ± 174.03	1420.82 ± 621.76
0.7	0.98 0.98 ± 0.05	18.47 17.52 ± 0.97	48.47 42.77 ± 5.14	8.76 7.35 ± 0.86	315.53 ± 110.12	1915.1 ± 712.39
0.9	0.93 0.90 ± 0.07	20.61 19.14 ± 1.31	54.06 45.24 ± 7.25	10.42 7.85 ± 1.90	252.11 ± 116.82	2143.24 ± 2067.07
1.1	0.96 0.99 ± 0.05	20.88 20.70 ± 0.43	57.68 48.70 ± 4.25	11.58 10.02 ± 0.99	167.73 ± 25.37	2502.31 ± 1187.69
1.3	0.95 0.94 ± 0.04	20.32 19.68 ± 0.73	56.04 49.79 ± 3.26	10.79 9.22 ± 0.91	162.69 ± 26.95	2036.76 ± 607.18

steady enhancement in PL intensity and narrowing of the emission profile, indicating improved film crystallinity and fewer trap-assisted recombination centers. However, at 1.3 mL/min, the PL intensity slightly decreases, suggesting the onset of over-crystallization or internal stress due to excessive solution wetting and delayed solvent removal. This interpretation is consistent with the XRD results presented earlier in Fig. 6(d). As discussed, residual PbI_2 peaks are observed at lower flow rates (0.5 and 0.7 mL/min), indicating incomplete conversion, while these peaks vanish above 0.9 mL/min, confirming complete transformation to the perovskite phase. Moreover, the sharpening of the (110) peak with increasing flow rate supports the observed PL trend of enhanced crystallinity. At 1.3 mL/min, while XRD still confirms full conversion, the slight PL decline highlights that excess flow may compromise uniformity despite phase purity. Together, these results reinforce that PL is a sensitive indicator of optoelectronic quality, and its correlation with XRD confirms the need to optimize the precursor flow rate for achieving both full conversion and high-performance perovskite films. This highlights the importance of balancing the deposition process: while an optimal flow rate enhances performance, exceeding this threshold can lead to over-crystallization or internal stress within the film, ultimately reducing efficiency. To investigate the effect of flow rates on the morphology of perovskite film, we perform atomic force microscopy (AFM) measurements to gain further insight into the morphology of perovskite using the various flow rates. According to the surface morphology shown in Fig. 7, lower flow rates resulted in a reduced concentration of organic salts, leading to non-uniform perovskite grain sizes. In contrast, higher flow rates facilitated the formation of more homogeneous perovskite films. At the same time, the root-mean-square (RMS) surface roughness of the perovskite films decreased from 43.34 nm to 20.27 nm as the flow rate increased from 0.5 mL/min to 1.1 mL/min. This reduction in surface roughness suggests an improvement in film compactness and smoothness, leading to enhanced interfacial contact between the perovskite layer and the electron transport layer (ETL). This enhanced contact facilitates more efficient charge extraction and transport, which correlates well with the observed improvement in J_{SC} and FF.

When comparing the performance of devices fabricated with three layers using R2S slot-die coating (including the HTL, inorganic, and organic layers) to those fabricated with spin-coating for all layers, the results demonstrate that transitioning from full spin-coating to partial R2S slot-die coating does not result in a significant decrease in device performance. In fact, the performance of devices with R2S coating is comparable to that of fully spin-coated devices, suggesting that the R2S process is highly successful in maintaining device efficiency. For devices with three layers coated using R2S (at a flow rate of 1.1 mL/min, the average PCE is 10.02 % (max: 11.58 %), V_{OC} is 0.99 V (max: 1.1 V), J_{SC} is 20.70 mA/cm^2 (max: 22.88 mA/cm^2), and FF is 48.70 % (max: 57.68 %). In contrast, devices made with spin-coating for all layers achieve an average PCE of 10.00 % (max: 13.24 %), V_{OC} of 1.07 V (max: 1.09 V), J_{SC} of 16.95 mA/cm^2 (max: 19.55 mA/cm^2), and FF of 55.14 % (max: 61.81 %). Although the devices fabricated using R2S for the three layers show

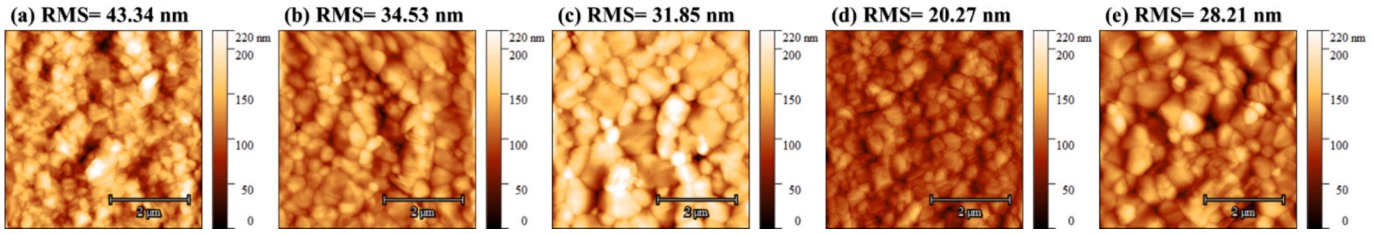

Fig. 7. AFM image of corresponding perovskite films with different flow rates. (a) 0.5 mL/min, (b) 0.7 mL/min, (c) 0.9 mL/min, (d) 1.1 mL/min, and (e) 1.3 mL/min.

slightly lower V_{OC} and FF values compared to the spin-coated devices, the overall PCE remains very similar, with only a small difference between the two methods. Furthermore, the maximum values achieved with R2S coating suggest that this method has the potential to achieve comparable or even better performance under optimized conditions. This comparison emphasizes that while spin-coating still provides the best performance in terms of V_{OC} and FF, the use of R2S slot-die coating for all layers is not detrimental to the device's performance. In fact, it shows promise for scalable production, as it offers uniformity and the potential for large-area coating processes. The results highlight that the R2S method, when optimized further, could serve as an effective alternative to spin-coating for fabricating high-efficiency devices. Therefore, the successful application of R2S slot-die coating for the three layers underlines its potential for both maintaining and improving the performance of photovoltaic devices in practical, large-scale production scenarios.

Previous experiments were conducted to establish the feasibility of using the R2S slot-die coating technique by validating the performance of small-area devices. Building upon these findings, we now extend our investigation to large-area coating, with a focus on validating the uniformity of the deposition process. Fig. 8(a) and (b) present the photograph and the PCE mapping of a 12 × 12 cm^2 substrate coated using the R2S slot-die coating technique, which involves the sequential deposition of three layers: the hole transport layer, an inorganic layer, and an organic layer. This mapping illustrates the distribution of PCE across different regions of the substrate, serving as a demonstration of the uniformity achieved in large-area coating. The results not only provide insights into the feasibility and advantages of scaling up this multi-layer deposition method but also emphasize the precision with which the R2S system can reproduce small-area deposition performance on larger substrates. The mapping results show that the overall PCE values range from 7.0 % to 11.0 %, with a relatively even distribution across the entire substrate. This uniformity is crucial for large-area solar cell fabrication, as it ensures consistent device performance across the entire area, addressing a common challenge in scaling up deposition techniques. Notably, the absence of large low-efficiency regions confirms that the R2S slot-die coating process is capable of maintaining stable coating quality over large areas, minimizing defects and ensuring uniform thin-film formation. These findings not only validate the scalability of the multi-layer deposition process but also highlight the potential of the R2S system to provide reliable, high-quality coatings in industrial-scale production. The successful translation from small-area to large-area processing underlines the system's robustness and its potential to meet the performance and efficiency requirements needed for commercial-scale solar cell manufacturing. This demonstrates the R2S platform's capacity for cost-effective, high-throughput fabrication, which is essential for the future of photovoltaic technologies.

To further elucidate the role of the wet-to-dry transition in the two-step R2S process, a direct control comparison was performed between devices fabricated with and without roller heating during the second-step organic-layer coating, while keeping all other processing parameters identical. This approach isolates the specific effect of thermal assistance on film formation, enabling a clear assessment of its influence on perovskite crystallization, film uniformity, and device performance. Applying roller heating resulted in more complete PbI_2-to-perovskite conversion, reduced grain size variation, and enhanced dark-storage stability, confirming that precise control of the wet-to-dry transition is a decisive factor in achieving high-performance flexible p–i–n perovskite solar cells. This comparison between R2S with and without heating in the second coating step provides strong evidence that thermal assistance is essential for achieving uniform and high-performance perovskite films. As shown in Fig. 9(a)–(d), all devices were fabricated with a fixed first-step heating temperature of 55 °C, while the second step was performed either with or without a heated roller. Devices processed with second-step heating exhibit significantly higher average values in V_{OC}, J_{SC}, FF, and PCE, along with much narrower data distributions. In contrast, devices fabricated without heating show large performance variation and generally poor efficiency, with some devices exhibiting

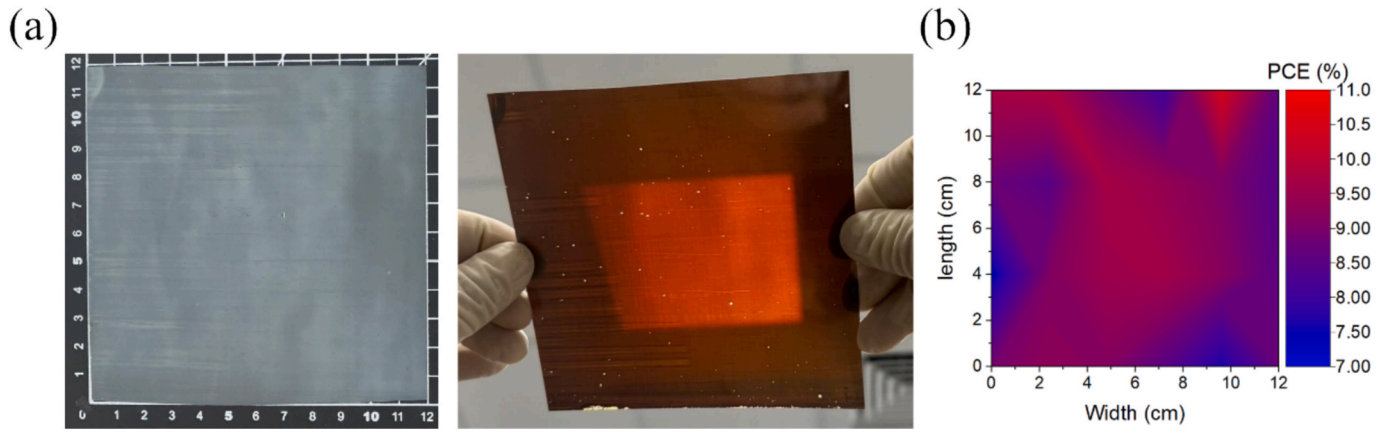

Fig. 8. A 12 × 12 cm^2 substrate coated using the R2S slot-die coating technique, with the hole transport layer, inorganic layer, and organic layer sequentially deposited. (a) Photograph of the resulting 12 × 12 cm^2 perovskite film. (b) The PCE values range from 7.0 % to 11.0 %, demonstrating uniformity across the substrate and validating the scalability of the deposition process.

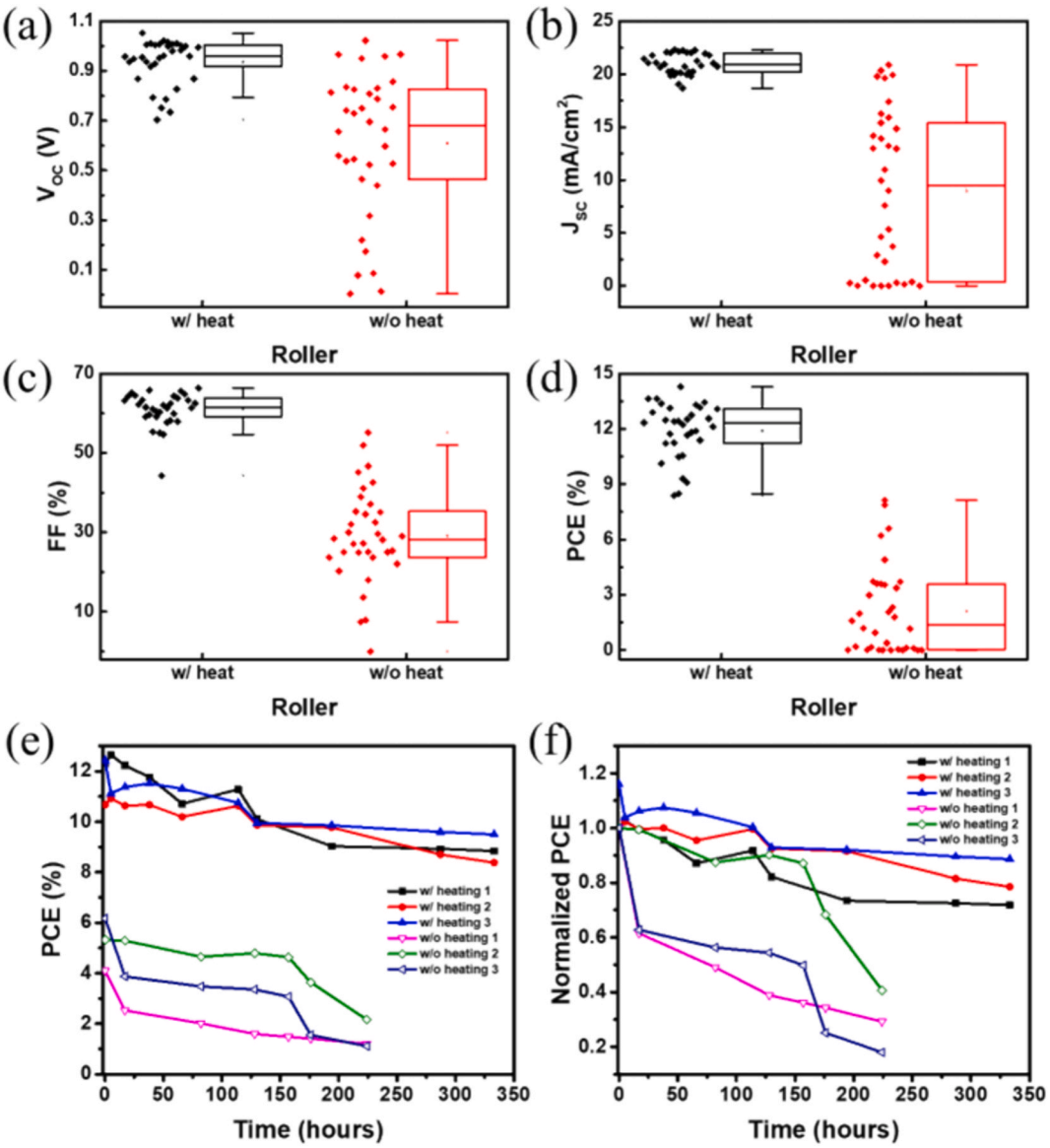

Fig. 9. Statistical analysis of photovoltaic parameters for perovskite solar cells fabricated via the R2S process with and without thermal assistance during the second coating step. (a) Open-circuit voltage (V_{OC}), (b) Short-circuit current density (J_{SC}), (c) Fill factor (FF), and (d) Power conversion efficiency (PCE). A constant first-step heating temperature of 55 °C was used for all samples. Devices processed with second-step heating exhibit significantly enhanced performance and reduced parameter variation, reflecting improved film quality and device reproducibility. (e) PCE and (f) normalized PCE of devices fabricated with (w/ heating) and without (w/o heating) roller heating during organic layer coating, measured under ambient conditions (25 °C, RH 40–50 %) in dark storage.

near-zero output. These results demonstrate that thermal control during the final drying stage improves solvent removal and crystallization, enhances process reliability, and ensures reproducibility, all of which are critical for scalable perovskite solar cell manufacturing. To assess operational robustness, we evaluated dark-storage stability of the flexible devices under ambient conditions (25 °C, RH 40–50 %) for over 300 h (Fig. 9(e)–(f)). Two fabrication conditions were examined: devices fabricated with roller heating applied during the organic-layer coating (w/ heating) and devices fabricated without roller heating (w/o heating). For each condition, three devices were tracked individually, and their stability trends are shown as separate curves. The w/ heating devices exhibit relatively consistent performance, retaining approximately 80 % of their initial PCE after >300 h. In contrast, the w/o heating devices degrade much faster, with all samples falling to <40 % of the initial PCE by ~220 h. These results demonstrate that applying roller heating during the organic-layer deposition yields a marked stability benefit, which we attribute to improved film morphology and interface quality under the optimized thermal condition.

5. Conclusions

This study validates the feasibility of our mechanism-informed roll-to-sheet (R2S) slot-die coating system, designed for uniform multi-layer deposition on large-area flexible substrates. The in-house developed W17RD15 platform integrates precise flow control and real-time thermal input via a heated roller, enabling consistent material distribution and reliable thin-film formation across flexible substrates. Compared to conventional spin-coating, this approach significantly improves material utilization and minimizes thickness variations, which are critical for uniform photovoltaic performance. The system allows flexible optimization of coating parameters to address challenges such as insufficient material coverage. For instance, by adjusting flow rates and coating strategies, the R2S system successfully achieved high-quality multi-layer films. Devices fabricated with two and three functional layers reached

power conversion efficiencies of up to 12.58 % and 11.58 %, respectively, which are comparable to the 13.24 % obtained via spin-coating. The integration of a heated roller not only enhances film uniformity and adhesion but also offers better control of crystallization and solvent evaporation kinetics, benefiting both organic and inorganic layer deposition. Furthermore, the R2S system demonstrated uniform 12 × 12 cm^2 coatings, highlighting its capability for large-area processing. Designed with scalability in mind, the W17RD15 platform enables process development and parameter optimization on a small scale before transitioning to full roll-to-roll production. With its precision, adaptability, and scalability, the R2S slot-die coating system offers a promising pathway toward industrial-scale, high-efficiency flexible photovoltaic manufacturing.

CRediT authorship contribution statement

Hou-Chin Cha: Writing – original draft, Investigation, Funding acquisition, Conceptualization. **Ssu-Yung Chung:** Validation, Formal analysis, Data curation. **Shih-Han Huang:** Validation, Formal analysis. **Chia-Feng Li:** Validation, Formal analysis. **Shun-Wei Liu:** Writing – review & editing, Resources, Project administration, Funding acquisition. **Yu-Ching Huang:** Writing – review & editing, Supervision, Resources, Project administration, Investigation, Funding acquisition, Conceptualization.

Declaration of competing interest

The authors declare that they have no known competing financial interests or personal relationships that could have appeared to influence the work reported in this paper.

Acknowledgments

The authors gratefully acknowledge the National Science and Technology Council for financial support (Grant Nos. NSTC-114-2222-E-131-002, 113-2221-E-131-021-MY3, 113-2622-E-131-009, 112-2622-E-131-011, 112-2628-E-131-001-MY4, and 112-2622-E-131-006). The corresponding author, S.-W. Liu, extends special thanks to Mr. Hsueh-Hsien Wu of Syskey Technology Co., Ltd. (Taiwan) for his critical contributions to the design of the fabrication chambers, which were instrumental in advancing this work. The authors also appreciate the support from Chang Gung University (Grant No. URRPD2N0011) and the Formosa Center at Ming Chi University of Technology (Grant No. FM002-113), both of which played a vital role in the successful completion of this research.

Appendix A. Supplementary data

Supplementary data to this article can be found online at https://doi.org/10.1016/j.solener.2025.113933.

References

[1] K. Sekar, R. Manisekaran, O.M. Nwakanma, M. Babudurai, Significance of formamidinium incorporation in perovskite composition and its impact on solar cell efficiency: a mini-review, Adv. Energy Sustain. Res. 5 (2024) 2400003.
[2] M.A. Green, A. Ho-Baillie, H.J. Snaith, The emergence of perovskite solar cells, Nat. Photonics 8 (2014) 506–514.
[3] J. Bing, L.G. Caro, H.P. Talathi, N.L. Chang, D.R. Mckenzie, A.W. Ho-Baillie, Perovskite solar cells for building integrated photovoltaics—glazing applications, Joule 6 (2022) 1446–1474.
[4] D. Angmo, G. DeLuca, A.D. Scully, A.S.R. Chesman, A. Seeber, C. Zuo, D. Vak, U. Bach, M. Gao, A lab-to-fab study toward roll-to-roll fabrication of reproducible perovskite solar cells under ambient room conditions, Cell Rep. Phys. Sci. 2 (2021) 100293.
[5] Y.Y. Kim, T.-Y. Yang, R. Suhonen, A. Kemppainen, K. Hwang, N.J. Jeon, J. Seo, Roll-to-roll gravure-printed flexible perovskite solar cells using eco-friendly antisolvent bathing with wide processing window, Nat. Commun. 11 (2020) 5146.
[6] M. Othman, F. Zheng, A. Seeber, A.S.R. Chesman, A.D. Scully, K.P. Ghiggino, M. Gao, J. Etheridge, D. Angmo, Millimeter-sized clusters of triple cation perovskite enables highly efficient and reproducible roll-to-roll fabricated inverted perovskite solar cells, Adv. Funct. Mater. 32 (2022) 2110700.
[7] H.C. Weerasinghe, N. Macadam, J.-E. Kim, L.J. Sutherland, D. Angmo, L.W.T. Ng, A.D. Scully, F. Glenn, R. Chantler, N.L. Chang, M. Dehghanimadvar, L. Shi, A.W. Y. Ho-Baillie, R. Egan, A.S.R. Chesman, M. Gao, J.J. Jasieniak, T. Hasan, D. Vak, The first demonstration of entirely roll-to-roll fabricated perovskite solar cell modules under ambient room conditions, Nat. Commun. 15 (2024) 1656.
[8] K. Poorkazem, D. Liu, T.L. Kelly, Fatigue resistance of a flexible, efficient, and metal oxide-free perovskite solar cell, J. Mater. Chem. A 3 (2015) 9241–9248.
[9] M. Soldera, Q. Wang, F. Soldera, V. Lang, A. Abate, A.F. Lasagni, Toward high-throughput texturing of polymer foils for enhanced light trapping in flexible perovskite solar cells using roll-to-roll hot embossing, Adv. Eng. Mater. 22 (2020) 1901217.
[10] C. Sílvia Manuela Ferreira, A.R. Luís, C.V. Júlio, Printing technologies on flexible substrates for printed electronics, in: R. Simas (Ed.), Flexible Electronics, IntechOpen, Rijeka, 2018 pp. Ch. 3.
[11] C.H. Chen, F. Hu, Z.H. Su, Y.J. Yu, K.L. Wang, Y.R. Shi, J. Chen, Y. Xia, X.Y. Gao, Z. K. Wang, Spring-like ammonium salt assisting stress release for low-temperature deposited FAPbI3 films toward flexible photovoltaic application, Adv. Funct. Mater. 33 (2023) 2213661.
[12] J.-I. Park, J.H. Heo, S.-H. Park, K.I. Hong, H.G. Jeong, S.H. Im, H.-K. Kim, Highly flexible InSnO electrodes on thin colourless polyimide substrate for high-performance flexible CH3NH3PbI3 perovskite solar cells, J. Power Sources 341 (2017) 340–347.
[13] Y. Gao, K. Huang, C. Long, Y. Ding, J. Chang, D. Zhang, L. Etgar, M. Liu, J. Zhang, J. Yang, Flexible perovskite solar cells: from materials and device architectures to applications, ACS Energy Lett. 7 (2022) 1412–1445.
[14] Y. Galagan, F. Di Giacomo, H. Gorter, G. Kirchner, I. de Vries, R. Andriessen, P. Groen, Roll-to-roll slot die coated perovskite for efficient flexible solar Cells, Adv. Energy Mater. 8 (2018) 1801935.
[15] B. Dou, J.B. Whitaker, K. Bruening, D.T. Moore, L.M. Wheeler, J. Ryter, N. J. Breslin, J.J. Berry, S.M. Garner, F.S. Barnes, Roll-to-roll printing of perovskite solar cells, ACS Energy Lett. 3 (2018) 2558–2565.
[16] J.-E. Kim, S.-S. Kim, C. Zuo, M. Gao, D. Vak, D.-Y. Kim, Humidity-tolerant roll-to-roll fabrication of perovskite solar cells via polymer-additive-assisted hot slot die deposition, Adv. Funct. Mater. 29 (2019) 1809194.
[17] J.F. Benitez-Rodriguez, D. Chen, A.D. Scully, C.D. Easton, D. Vak, H. Li, P.E. Shaw, P.L. Burn, R.A. Caruso, M. Gao, Slot-die coating of a formamidinium-cesium mixed-cation perovskite for roll-to-roll fabrication of perovskite solar cells under ambient laboratory conditions, Sol. Energy Mater. Sol. Cells 246 (2022) 111884.
[18] K. Hwang, Y.-S. Jung, Y.-J. Heo, F.H. Scholes, S.E. Watkins, J. Subbiah, D.J. Jones, D.-Y. Kim, D. Vak, Toward large scale roll-to-roll production of fully printed perovskite solar cells, Adv. Mater. 27 (2015) 1241–1247.
[19] Y.-J. Heo, J.-E. Kim, H. Weerasinghe, D. Angmo, T. Qin, K. Sears, K. Hwang, Y.-S. Jung, J. Subbiah, D.J. Jones, Printing-friendly sequential deposition via intra-additive approach for roll-to-roll process of perovskite solar cells, Nano Energy 41 (2017) 443–451.
[20] H. Li, C. Zuo, D. Angmo, H. Weerasinghe, M. Gao, J. Yang, Fully roll-to-roll processed efficient perovskite solar cells via precise control on the morphology of PbI2: CsI layer, Nano-Micro Lett. 14 (2022) 79.
[21] Y.-C. Huang, H.-C. Cha, C.-Y. Chen, C.-S. Tsao, Morphological control and performance improvement of organic photovoltaic layer of roll-to-roll coated polymer solar cells, Sol. Energy Mater. Sol. Cells 150 (2016) 10–18.
[22] C.-Y. Chang, Y.-C. Huang, C.-S. Tsao, W.-F. Su, Formation mechanism and control of perovskite films from solution to crystalline phase studied by in situ synchrotron scattering, ACS Appl. Mater. Interfaces 8 (2016) 26712–26721.
[23] B.-J. Huang, C.-K. Guan, S.-H. Huang, W.-F. Su, Development of once-through manufacturing machine for large-area Perovskite solar cell production, Sol. Energy 205 (2020) 192–201.
[24] G.Y. Park, M.-J. Kim, J.Y. Oh, H. Kim, B. Kang, S.-K. Cho, W.J. Choi, M. Kim, D. S. Ham, High-throughput roll-to-roll processed large-area perovskite solar cells using rapid radiation annealing technique, ACS Appl. Mater. Interfaces (2024).
[25] Y.-C. Huang, C.-F. Li, Z.-H. Huang, P.-H. Liu, C.-S. Tsao, Rapid and sheet-to-sheet slot-die coating manufacture of highly efficient perovskite solar cells processed under ambient air, Sol. Energy 177 (2019) 255–261.
[26] S.-H. Huang, C.-K. Guan, P.-H. Lee, H.-C. Huang, C.-F. Li, Y.-C. Huang, W.-F. Su, Toward all slot-die fabricated high efficiency large area perovskite solar cell using rapid near infrared heating in ambient air, Adv. Energy Mater. 10 (2020) 2001567.